WDR91 is a Rab7 effector required for neuronal development

Kai Liu,[1,4]* Ruxiao Xing,[1,2]* Youli Jian,[1]* Zhiyang Gao,[1]* Xinli Ma,[2,3] Xiaojuan Sun,[1] Yang Li,[1] Meng Xu,[1] Xin Wang,[1,4] Yudong Jing,[1] Weixiang Guo,[1] and Chonglin Yang[1,4]

[1]State Key Laboratory of Molecular and Developmental Biology, Institute of Genetics and Developmental Biology, [2]Graduate University of and [3]Institute of Biophysics, Chinese Academy of Sciences, Beijing, China
[4]State Key Laboratory of Natural Resource Conservation and Utilization in Yunnan and Center for Life Science, School of Life Sciences, Yunnan University, Kunming, China

Early-to-late endosome conversion, which is essential for delivery of endosomal cargoes to lysosomes, requires switching of early endosome–specific Rab5 and PtdIns3P to late endosome–specific Rab7 and PtdIns(3,5)P_2. In this study, we identify the WD40-repeat protein WDR91 as a Rab7 effector that couples Rab switching with PtdIns3P down-regulation on endosomes. Loss of WDR91 greatly increases endosomal PtdIns3P levels, arresting endosomes at an intermediate stage and blocking endosomal–lysosomal trafficking. WDR91 is recruited to endosomes by interacting with active guanosine triphosphate–Rab7 and inhibits Rab7-associated phosphatidylinositol 3-kinase activity. In mice, global *Wdr91* knockout causes neonatal death, whereas brain-specific *Wdr91* inactivation impairs brain development and causes postnatal death. Mouse neurons lacking *Wdr91* accumulate giant intermediate endosomes and exhibit reduced neurite length and complexity. These phenotypes are rescued by WDR91 but not WDR91 mutants that cannot interact with Rab7. Thus, WDR91 serves as a Rab7 effector that is essential for neuronal development by facilitating endosome conversion in the endosome–lysosome pathway.

Introduction

Endosome–lysosome trafficking, which requires sequential and coordinated actions of endosomes and lysosomes, is central to cell homeostasis by supplying nutrients, modulating the magnitude of signals, and providing membranes for membrane repair, cell migration, and neurite outgrowth (Ascano et al., 2012; Irannejad et al., 2015; Maritzen et al., 2015). Adequate early-to-late endosome conversion is a key step for successful delivery of endosomal cargoes to the lysosome (Rink et al., 2005; Cabrera and Ungermann, 2010; Huotari and Helenius, 2011). Early endosomes are specified by the Rab5 small GTPase and phosphatidylinositol 3-phosphate (PtdIns3P). Late endosomes, on the other hand, are characterized by the Rab7 small GTPase and phosphatidylinositol 3,5-biphosphate (PtdIns(3,5)P_2; Ikonomov et al., 2006; Numrich and Ungermann, 2014). Thus, the conversion of early endosomes to late endosomes requires the switching of Rab5 to Rab7 and PtdIns3P to PtdIns(3,5)P_2.

It is now understood that a complex containing Mon1/SAND-1 and Ccz1/CCZ-1 controls the replacement of Rab5 with Rab7 on endosomes (Nordmann et al., 2010; Poteryaev et al., 2010). By sensing the membrane PtdIns3P levels and the size of early endosomes, Mon1/SAND-1 localizes to early endosomes, where it displaces the guanine nucleotide exchange factor of Rab5, Rabex-5/RABX-5, thus preventing the continuous activation of Rab5 (Poteryaev et al., 2010). In the meantime, Mon1/SAND-1 forms a complex with Ccz1/CCZ-1, which functions as the guanine nucleotide exchange factor of Rab7 to promote its activation and membrane enrichment (Nordmann et al., 2010; Cabrera et al., 2014; Shinde and Maddika, 2016). The active GTP-bound Rab7 (GTP-Rab7) can recruit TBC-2, a Rab5 GTPase–activating protein, to help to inactivate GTP-bound Rab5 (GTP-Rab5; Li et al., 2009; Chotard et al., 2010). Unlike the process of Rab5-to-Rab7 switching, however, the mechanism that determines how endosomal PtdIns3P is down-regulated to allow the necessary change of lipid identity is not well understood. Endosomal PtdIns3P is generated by the class III phosphatidylinositol 3-kinase (PI3K) complex, which consists of Vps34, p150/Vps15, and Beclin1/Atg6 (Christoforidis et al., 1999; Funderburk et al., 2010). Intriguingly, both Rab5 and Rab7 are implicated in the regulation of endosomal PtdIns3P levels. The active GTP-Rab5 was shown to promote endosomal association of the PI3K complex by interacting with p150/Vps15, thus facilitating generation of PtdIns3P on endosomes (Christoforidis et al., 1999; Murray et al., 2002). Rab7 was also found to interact with p150/Vps15, forming a complex exclusive of Rab5 (Stein et al., 2003, 2005).

*K. Liu, R. Xing, Y. Jian, and Z. Gao contributed equally to this paper.

Correspondence to Chonglin Yang: clyang@genetics.ac.cn; Weixiang Guo: wxguo@genetics.ac.cn

Abbreviations used: cKO, conditional KO; EGFR, EGF receptor; IP, immunoprecipitation; KO, knockout; PI3K, phosphatidylinositol 3-kinase; PtdIns3P, phosphatidylinositol 3-phosphate.

The Rockefeller University Press
J. Cell Biol. Vol. 216 No. 10 3307–3321
https://doi.org/10.1083/jcb.201705151

However, given that PtdIns3P is most abundant on early endosomes and early endosomal carrier vesicles but is not obviously seen on late endosomes/multivesicular bodies (Gillooly et al., 2000), it is unclear how the interaction of Rab7 with the PI3K complex affects its activity and hence the change of PtdIns3P levels on endosomes, particularly in the process of early-to-late endosome conversion.

Recently, our work identified two previously unknown factors, SORF-1 and SORF-2, which negatively regulate endosomal PtdIns3P for early-to-late endosome conversion in *Caenorhabditis elegans* (Liu et al., 2016). SORF-1 and SORF-2 form a complex with Beclin1 and inhibit the activity of the PI3K complex. In mammalian cells, WDR91 and WDR81, the homologues of *C. elegans* SORF-1 and SORF-2, respectively, also form a complex with Beclin1. Intriguingly, WDR91 differs from *C. elegans* SORF-1 in that it contains an additional WD40-repeat region in the C terminus (Liu et al., 2016). This suggests that WDR91 and *C. elegans* SORF-1 might be regulated differently, though both of them were shown to inhibit PtdIns3P generation (Liu et al., 2016). It is not known how WDR91 executes its functions on endosomes. Moreover, the requirement for WDR91 in endosomal trafficking and mammalian development is not currently understood. In the present study, we investigate the role of WDR91 in the endosome–lysosome pathway. We find that loss of WDR91 impairs early-to-late endosome conversion, resulting in accumulation of giant intermediate endosomes and defective endosomal delivery of diverse cargoes to the lysosome. We demonstrate that WDR91 is recruited to endosomes by directly interacting with active Rab7, and the interaction of WDR91 with the active GTP-Rab7 is required to inhibit the activity of the Rab7-associated PI3K complex. This allows the turnover of endosomal PtdIns3P and consequently conversion of early endosomes to late endosomes. Moreover, we show that WDR91 is essential for neonatal survival and postnatal brain development in mice. Depletion of *Wdr91* prevents efficient endosome conversion in neurons, leading to defective dendritic arborization and reduced brain size. Our findings thus uncover a new Rab7 effector that is important for neuronal development by facilitating early-to-late endosome conversion in the endosome–lysosome pathway.

Results

Inactivation of WDR91 causes PtdIns3P-dependent trapping of intracellular cargoes in endosomes

To investigate the requirement for WDR91 in endosomal trafficking, we examined the delivery of endocytic cargoes to the lysosome in *WDR91* knockout (KO; KO-91) HeLa cells (Liu et al., 2016). First, we performed time course monitoring of the trafficking of EGF receptor (EGFR). In control HeLa cells, EGFR was enriched on EEA1-positive early endosomes 15 min after the treatment of cells with EGF, and this enrichment was progressively and strongly decreased at 45 and 90 min (Fig. 1, A and B). As the EGFR signal decreased on EEA1 endosomes, it became enriched on LAMP1-positive lysosomes at corresponding time points (Fig. 1, C and D). In KO-91 cells, EGFR was similarly enriched on the enlarged EEA1 endosomes 15 min after EGF treatment; however, it remained on these endosomes even 90 min after EGF treatment (Fig. 1, A and B). The colocalization of EGFR with LAMP1 was much lower in KO-91 cells than in control cells at all time points examined (Fig. 1, C and D). Next, we examined endosome–lysosome transport of fluorescently labeled dextran, which was endocytosed by macropinocytosis. Cells were incubated with dextran 405 for 30 min to allow for endocytic uptake and then left for 1.5 h after removal of dextran to allow for endosomal trafficking. In control cells, dextran was enriched in EEA1-positive endosomes after 30-min incubation and appeared in LAMP1-positive vesicles 1.5 h later. In KO-91 cells, however, most of the dextran signal was seen in EEA1 endosomes, and no dextran appeared in LAMP1-positive lysosomes after the further 1.5-h incubation (Fig. 1 E). These results indicate that inactivation of WDR91 impaired transport of intracellular cargoes from endosomes to lysosomes.

We investigated whether the defective endosomal trafficking results from elevated endosomal PtdIns3P in KO-91 cells. We treated cells with VPS34-IN1, a specific inhibitor of Vps34, and found that EGFR efficiently exited from EEA1 endosomes and appeared in LAMP1-positive lysosomes in KO-91 cells, just like in control cells (Fig. 1, F–H). This suggests that the increase in endosomal PtdIns3P is responsible for the defective transport of intracellular cargoes to the lysosome in KO-91 cells.

Loss of WDR91 leads to defective early-to-late endosome conversion

To understand how the increase in endosomal PtdIns3P compromises endosomal delivery of cargoes to the lysosome, we attempted to determine the identity of the enlarged endosomes in KO-91 cells using immunostaining assays. In control cells, a low level of colocalization between Rab7 or LAMP1 and 2×FYVE-GFP, which labels PtdIns3P, was detected (Fig. 2, A and B). In KO-91 cells, however, a strong increase in the colocalization of 2×FYVE-GFP with Rab7 on the enlarged endosomes was observed, whereas the colocalization of 2×FYVE-GFP with LAMP1 remained at a similar level to control cells (Fig. 2, A and B). Similarly, the early endosomal protein EEA1 colocalized with Rab7 to the enlarged endosomes in KO-91 cells, and the extent of colocalization was much higher than in control cells (Fig. 2, C and D). In addition, both EEA1 and the early endosome–specific Rab5 GTPase were found to colocalize strongly with the late endosome–specific Rab9 GTPase to the enlarged endosomes in KO-91 cells (Fig. S1, A and C). The enlarged endosomes in KO-91 cells were negative for LAMP1, the ER protein Sec61-β, and the TGN protein p230 (Fig. 2 C and Fig. S1, B and C). Together, these findings suggest that these enlarged endosomes, which are positive for PtdIns3P, early endosomal proteins, and late endosomal proteins, are intermediates in early-to-late endosome conversion. To consolidate this conclusion, we performed live-cell imaging to monitor the endosome conversion process. In control cells, the early endosomal and PtdIns3P indicator 2×FYVE-mCherry (2×FYVE-mCh) progressively disappeared, and the late endosome–specific Rab7 (GFP-Rab7) gradually appeared on endosomes, indicating the conversion of early endosomes to late endosomes. The duration of intermediate endosomes colabeled with these two markers was <6 min (Fig. 2, E and G; and Video 1). In KO-91 cells, 2×FYVE-mCh first appeared and persisted on the enlarged endosomes, and Rab7 was subsequently corecruited. The duration of the intermediate endosomes was >60 min, and no completion of endosome conversion was observed during the monitoring period (Fig. 2, F and G; and Video 2). Importantly, inhibition of PtdIns3P generation by VPS34-IN1 or siRNA knockdown of Beclin1 strongly suppressed the formation of the enlarged

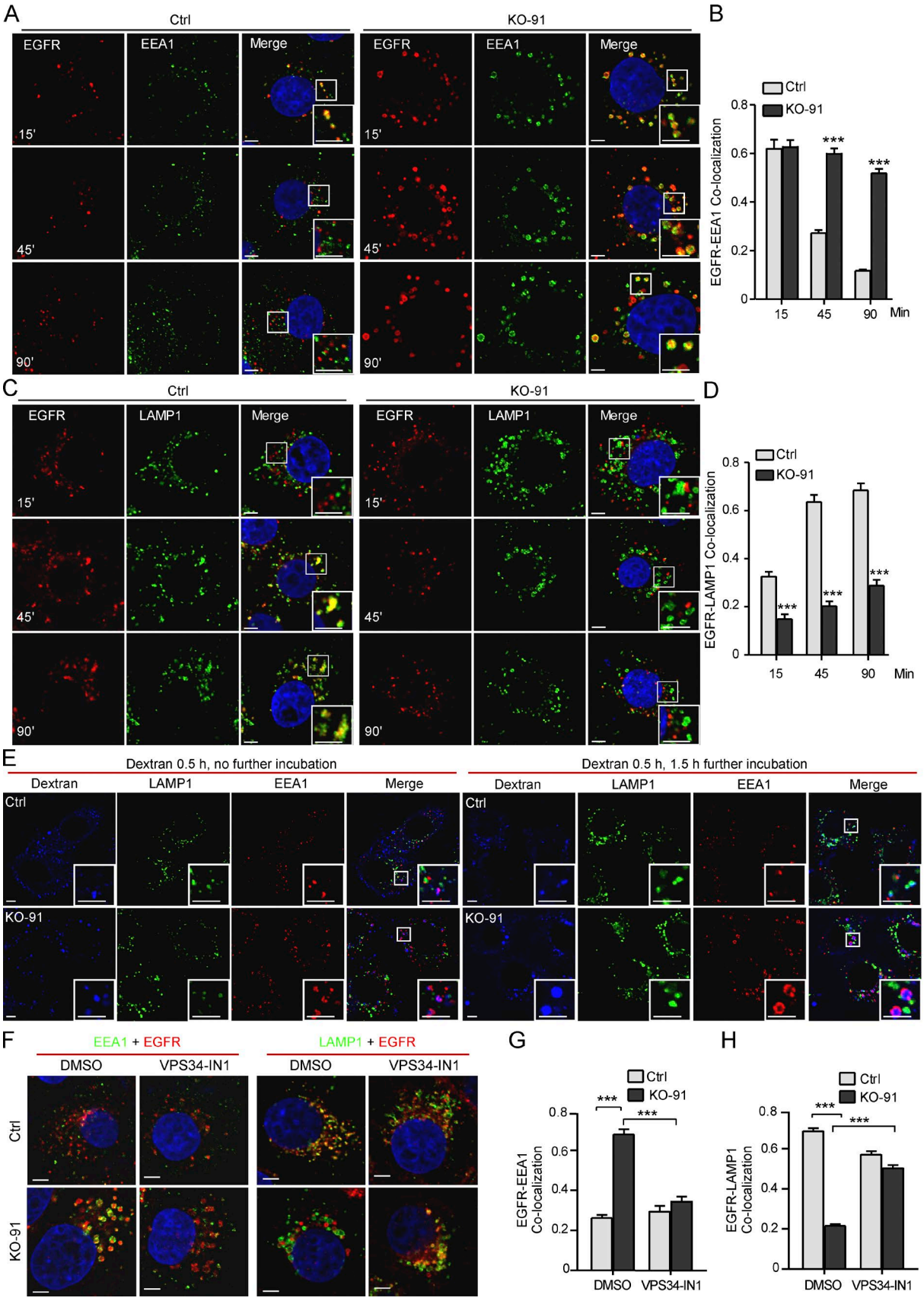

Figure 1. **Loss of *WDR91* causes PtdIns3P-dependent endosomal trafficking defects.** (A) Coimmunostaining of cells with EGFR and EEA1. Control and KO-91 HeLa cells were fixed and stained at the indicated time points after 25 ng/ml EGF stimulation. (B) Quantification of EGFR-EEA1 colocalization at the indicated time points after EGF stimulation. (C) Coimmunostaining of cells with EGFR and LAMP1. Cells were treated as in A. (D) Quantification of

intermediate endosomes positive for both EEA1 and Rab7 in KO-91 cells (Fig. 2, H and I). Collectively, these findings indicate that loss of WDR91 function led to an elevation in endosomal PtdIns3P levels, which in turn caused defective early-to-late endosome conversion and resulted in defective endosome–lysosome trafficking.

WDR91 is recruited to endosomes by active Rab7

We next investigated whether WDR91 executes its function on endosomes. Using immunostaining, we found that only a small proportion of endogenous WDR91 colocalized with EEA1, whereas most WDR91 was colocalized with Rab7 or LAMP1 (Fig. 3, A and B). In coexpression assays, GFP-WDR91 mainly colocalized with mCherry-tagged late endosomal proteins Rab7 (mCh-Rab7), Rab9 (mCh-Rab9), and CD63 (mCh-CD63) but not mCherry-fused early endosomal proteins EEA1 (mCh-EEA1) and Rab5 (mCh-Rab5; Fig. S1 D). GFP-WDR91 localized to a proportion of LAMP1-mCherry (LAMP-mCh)–marked vesicles, and it did not localize to LysoTracker-positive lysosomes (Fig. S1 D). In addition, GFP-WDR91 did not colocalize with the mCherry-tagged ER protein Sec61β (mCh-Sec61β; Fig. S1 D). Together, these data suggest that WDR91 is mainly located on late endosomes. Because WDR91 does not have an obvious transmembrane domain, we examined whether WDR91 interacts with endosomal Rab GTPases, including Rab5, Rab7, and Rab9. Using immunoprecipitation (IP) assays, we found that GFP-Rab7 but not Rab5 or Rab9 was coprecipitated with Flag-WDR91 (Fig. 3 C). These results suggest that WDR91 specifically interacts with Rab7. We next investigated whether the localization of WDR91 to endosomes is dependent on Rab7. siRNA knockdown of Rab7 strongly reduced the colocalization of endogenous WDR91 with Rab9 (Fig. 3, D–F). siRNA of Rab7 similarly reduced the colocalization of GFP-WDR91 with mCh-CD63 (Fig. S1 E). In addition, WDR91 was found to localize to EGFR-positive endosomes 15 min after EGF treatment; however, siRNA of Rab7 greatly decreased WDR91 localization on EGFR endosomes (Fig. S1 F). Collectively, these findings suggest that the recruitment of WDR91 to endosomes is dependent on Rab7.

Rab7 switches between the active membrane-associated, GTP-bound form and the inactive cytosolic GDP-bound form. We next investigated whether WDR91 preferentially interacts with GTP- or GDP-bound Rab7. In co-IP assays, Flag-WDR91 interacted with GFP-tagged WT Rab7 (GFP-Rab7) and Rab7(Q67L), the GTP-bound and constitutively active form of Rab7. No obvious interaction was detected between Flag-WDR91 and GFP-Rab7(T22N), the GDP-bound and constitutively inactive form of Rab7, in the same co-IP assays (Fig. 3 G). In vitro, GST-Rab7 directly pulled down ^{35}S-labeled WDR91 (Fig. 3 H). The interaction of ^{35}S-WDR91 with GST-Rab7(Q67L) in the presence of GTP was much stronger, whereas the interaction of ^{35}S-WDR91 with GST-Rab7(T22N) was much weaker in the presence of GDP (Fig. 3 H). These results indicate that WDR91 interacts with the active GTP-Rab7. Confirming this conclusion, we observed a robust colocalization between Flag-WDR91 and mCh-CD63 when they were coexpressed with BFP-tagged Rab7 or Rab7(Q67L) in HeLa cells (Fig. 3 I). In contrast, the colocalization of Flag-WDR91 with mCh-CD63 was mostly abolished when they were coexpressed with BFP-Rab7(T22N) (Fig. 3 I). Collectively, these findings suggest that WDR91 is a Rab7 effector that is recruited to endosomes by the active form of Rab7.

Characterization of the WDR91–Rab7 interaction

WDR91 contains seven putative WD40 repeats at the C terminus (aa 392–741) and a coiled-coil domain (aa 178–215) in the N terminus (Fig. 4 A). Both WD40 repeats and the coiled-coil domain are involved in protein–protein interactions. To determine which domain in WDR91 is responsible for the interaction with Rab7, we generated GFP-tagged WDR91 truncations (Fig. 4 A) and tested their interaction with Flag-Rab7 using co-IP assays. Full-length WDR91 and WDR91(392–747), which contain all seven WD40 repeats, were coimmunoprecipitated with Flag-Rab7 (Fig. 4 B). In contrast, WDR91(1–405) containing the coiled-coil domain did not interact with Flag-Rab7 (Fig. 4 B). Interestingly, WDR91(1–700) and WDR91(518–747), which are devoid of the last and the first two WD40 repeats, respectively, did not interact with Rab7 in the same co-IP assays (Fig. 4 B). Using in vitro GST pull-down assays, we found that GST-Rab7 interacted with ^{35}S-labeled full-length WDR91 and WDR91(392–747) but not WDR91(1–405) (Fig. 4 C). Collectively, these data suggest that WDR91 directly interacts with Rab7 through the intact WD40-repeat region. In addition, we found that GFP-WDR91(1–405) but not GFP-WDR91(392–747) coimmunoprecipitated with HA-tagged Beclin1 (Fig. 4 D). Furthermore, GFP-WDR91(1–218) and WDR91(219–405) were also coprecipitated with HA-Beclin1 (Fig. 4 D), suggesting that Beclin1 possibly binds to multiple sites in the N terminus of WDR91. Thus, Beclin1 and Rab7 bind to the N and C termini of WDR91, respectively.

We next investigated whether WDR91(392–747) interacts with GTP-Rab7 but not GDP-Rab7, like full-length WDR91. In co-IP assays, GFP-tagged Rab7 and Rab7(Q67L), but not Rab7(T22N), were coimmunoprecipitated with Flag-WDR91 (Fig. 4 E). No obvious interaction was detected between Flag-WDR91(1–405) and any Rab7 forms; however, Flag-WDR91(392–747) interacted equally well with all forms of Rab7 (Fig. 4 E). Similarly, whereas the interaction of full-length WDR91 with GST-Rab7(Q67L) in the presence of GTP was much stronger than the interaction with GST-Rab7(T22N) in the presence of GDP in GST pull-down assays, WDR91(392–747) interacted equally well with GST-Rab7(Q67L) and GST-Rab7(T22N) in the same assays, and no direct interaction was detected between WDR91(1–405) and either form of GST-Rab7 (Fig. 4 F). These data suggest that although the intact WD40 repeats are sufficient and necessary to interact with Rab7, the

EGFR-LAMP1 colocalization in cells from C. Data are plotted as in B. (E) Confocal images of dextran 405 in control and KO-91 HeLa cells costained with EEA1 and LAMP1. Cells were incubated with dextran 405 for 30 min and then fixed immediately or after incubation without dextran for a further 1.5 h. (F) Coimmunostaining of EGFR with EEA1 (left) or LAMP1 (right) in control and KO-91 HeLa cells 60 min after EGF stimulation. Cells were treated without or with 500 nM VPS34-IN1 for 3 h. Insets show magnified views of the box in the merged images. Bars, 5 µm. (G and H) Quantification of the colocalization of EGFR with EEA1 (G) and EGFR with LAMP1 (H) as shown in F. For all quantifications, Pearson's correlation coefficient is plotted on the y-axis. ≥50 cells were scored. Error bars represent SEM. ***, $P < 0.001$.

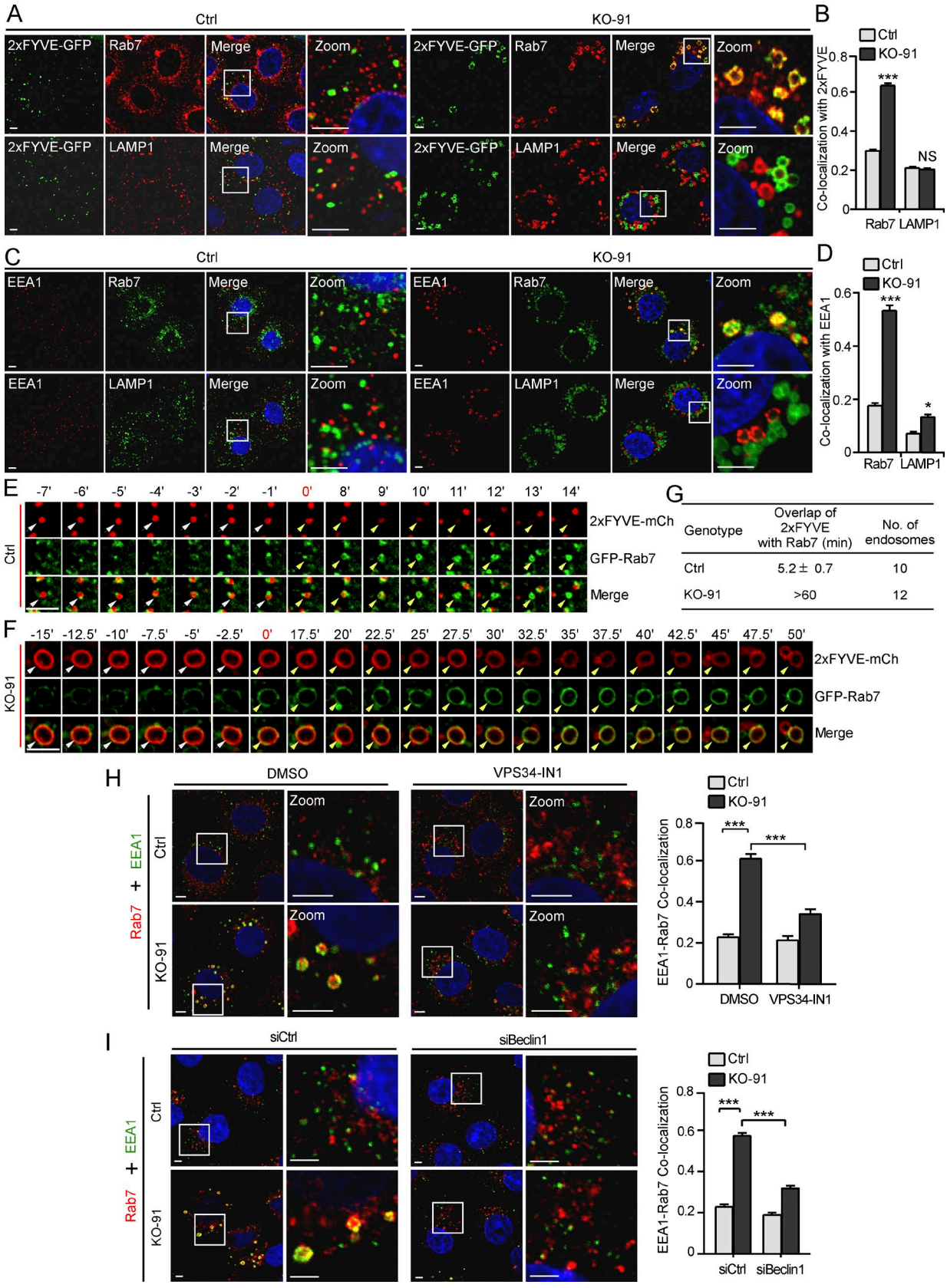

Figure 2. **Loss of WDR91 leads to accumulation of endosomal PtdIns3P and defective early-to-late endosome conversion.** (A) Colocalization of 2×FYVE-GFP with endogenous Rab7 or LAMP1 in control and KO-91 HeLa cells. Bars, 5 µm. (B) Quantification of the colocalization of endosomal/lysosomal markers as shown in A. (C) Colocalization of endogenous EEA1 with Rab7 or LAMP1 in control and KO-91 HeLa cells. Bars, 5 µm. (D) Quantification of the colocalization of endosomal/lysosomal proteins as shown in C. (E and F) Time-lapse recording of dynamic changes of the early endosomal marker 2×FYVE-mCh and the late endosomal protein GFP-Rab7 on endosomes in control (E) and KO-91 (F) HeLa cells. Cells were imaged 24 h after transfection. 0 min

N terminus of WDR91 is needed to confer the specificity to interact with the active GTP-Rab7.

We then sought to determine the key amino acid residues in the WD40-repeat domain that are required for WDR91–Rab7 interaction. Structural modeling using the Phyre2 server (Kelley et al., 2015) revealed that WDR91(392–747) exhibits a putative, classical seven-bladed β-propeller architecture, with each blade comprising a four-stranded, antiparallel β sheet (Fig. S2, A–C). Given that WD40-repeat domains usually interact with their protein partners through the top or bottom surface of the β propeller (Stirnimann et al., 2010), we mutated solvent-exposed surface residues on the top and bottom loops of each repeat and examined the colocalization of these WDR91 mutants with mCh-Rab7. Among the eight mutants we tested, only F570A/N571A/H572A (3A) failed to colocalize with mCh-Rab7 (Fig. 4 G and Fig. S2 D). F570, N571, and H572 are highly conserved among diverse species (Fig. S2 E) and are located on the interaction surface of the putative WDR91–Rab7 complex model (Fig. S2 F) built on the basis of the structure of a complex containing the RAN small GTPase and RCC1, a seven-bladed propeller protein (Renault et al., 2001). In co-IP assays, the Flag-WDR91(3A) mutant failed to associate with GFP-Rab7(Q67L) but was coprecipitated with Beclin1 (Fig. 4, H and I). Together, these findings suggest that F570, N571, and H572 in the WD40-repeat domain are essential for WDR91 to interact with Rab7.

We also attempted to identify residues in the N terminus that are important for determining the interaction specificity between WDR91 and GTP-Rab7. A sequence alignment revealed that a string of amino acid residues in WDR91 (aa 159–163) is highly conserved across diverse species ranging from *C. elegans* to humans (Fig. S2 G). We thus deleted these five residues and found that the resulting WDR91(Δ5) mutant tagged with Flag failed to colocalize mCh-Rab7 (Fig. 4 G). In co-IP assays, Flag-WDR91(Δ5) did not coprecipitate with GFP-Rab7(Q67L), whereas it still associated with Beclin1 (Fig. 4, H and I). Thus, the N-terminal amino acids 159–163 are essential for endowing WDR91 with the specificity to interact with the active GTP-Rab7.

Inhibition of endosomal PI3K activity by WDR91 depends on the WDR91–Rab7 interaction

Our findings suggest that WDR91 is recruited to endosomes by directly interacting with active Rab7. Because WDR91 also interacts with Beclin1 (Liu et al., 2016), we examined whether WDR91 associates with the endosomal or autophagic PI3K complex. In co-IP assays with Beclin1 antibody, WDR91, Rab7, Vps34, and Atg14L were coimmunoprecipitated with Beclin1. Using antibodies to WDR91 and Rab7 for coIPs, WDR91 and Rab7 were reciprocally coimmunoprecipitated with one another, and Vps34 and Beclin1 were coprecipitated with them (Fig. 5 A). However, the autophagy-specific ATG14L did not associate with either WDR91 or Rab7 in the same co-IP assays (Fig. 5 A). These findings suggest that WDR91 associates specifically with the endosomal PI3K complex. We next assessed the effect of WDR91 on the endosomal PI3K complex by immunoprecipitating Rab7-associated PI3K complexes and measuring their activities. As shown in Fig. 5 B, the Rab7-associated PI3K complex from KO-91 showed significantly higher activity than that from control HeLa cells, suggesting that WDR91 suppresses the activity of the endosomal PI3K complex. We then investigated whether the inhibitory effect of WDR91 on endosomal PI3K requires the interaction with Rab7. We coexpressed GFP-Rab7(Q67L) with Flag-WDR91, WDR91(3A), or WDR91(Δ5). After IP, we measured the PI3K activity associated with GFP-Rab7(Q67L). Flag-WDR91 was coprecipitated with GFP-Rab7(Q67L) and reduced the endosomal PI3K activity in KO-91 cells to a level similar to that in control cells (Fig. 5 C). Flag-WDR91(3A) and Flag-WDR91(Δ5), however, did not associate with GFP-Rab7(Q67L) and failed to suppress the increase in endosomal PI3K activity in KO-91 cells (Fig. 5 C). Using a PtdIns3P antibody, we confirmed that the strongly increased endosomal PtdIns3P was rescued by Flag-WDR91 but not Flag-WDR91(3A) and Flag-WDR91(Δ5) (Fig. 5, D and E). Consistent with this, expression of Flag-WDR91 in KO-91 cells, but not Flag-WDR91(3A) or Flag-WDR91(Δ5), prevented the formation of enlarged EEA1 endosomes containing trapped EGF or dextran 405 (Fig. 5, F–H; and Fig. S3). Collectively, these findings suggest that WDR91 inhibits endosomal PI3K activity in a manner that depends on the interaction with Rab7. Thus, WDR91 maintains normal early-to-late endosome conversion and hence endosome–lysosome trafficking within the cell.

Wdr91 KO impairs dendritic arborization during postnatal development of the mouse brain

Given that WDR91 functions as a Rab7 effector in endosome–lysosome trafficking, we asked whether WDR91 plays an important role in mammalian development. In mice, *Wdr91* gene expression was detected in many tissues (Fig. S4 A). We generated *Wdr91* KO mice by replacing a part of the sequence of exons 2–6 in the *Wdr91* gene with a nucleus-localized β galactosidase (nLacZ) cassette (Fig. S4 B). This leads to disruption of *Wdr91* gene expression while simultaneously enabling detection of endogenous *Wdr91* expression. *Wdr91* KO mice were born at the expected Mendelian frequency but died quickly after birth with intraabdominal bleeding as judged by autopsy (Fig. S4 C). In the brain, nLacZ was mainly detected in neurons that were positive for NeuN staining but not in glial cells that were stained with S100-β (Fig. S4 D). This suggests that WDR91 likely plays an important role in neuronal function or development. Because *Wdr91* shows the highest expression in the brain (Fig. S4 A), we next generated *Wdr91*-floxed mice with LoxP sites flanking exon 3 and then crossed these animals with mice expressing the Cre recombinase driven by the promoter of the brain-abundant *Nestin* gene (*Nestin-Cre*). Thus, we obtained *Wdr91$^{f/f}$*:*Nestin-Cre* (*Wdr91* conditional KO [cKO]) mice (Fig.

refers to the time point when GFP-Rab7 was fully recruited on 2×FYVE-mCh–positive endosomes. White and yellow arrows indicate the followed endosomes before and after enrichment of GFP-Rab7, respectively. Bars, 3 µm. (G) Duration of the overlap of 2×FYVE and Rab7 on endosomes as shown in E and F. (H) Colocalization of EEA1 with Rab7 in control and KO-91 HeLa cells treated without or with 500 nM VPS34-IN1 for 3 h. Bars, 5 µm. Quantification of colocalization is shown on the right. (I) Colocalization of EEA1 with Rab7 in control and KO-91 HeLa cells treated with control siRNA (siCtrl) or Beclin1 siRNA (siBeclin1). Zoom images represent magnified views of boxed areas. Quantification of colocalization is shown on the right. For all quantifications, ≥50 cells were scored. The y-axis shows the value of Pearson's correlation coefficient. Error bars represent SEM. *, $P < 0.05$; ***, $P < 0.001$. Images shown in E and F were derived from Videos 1 and 2, respectively.

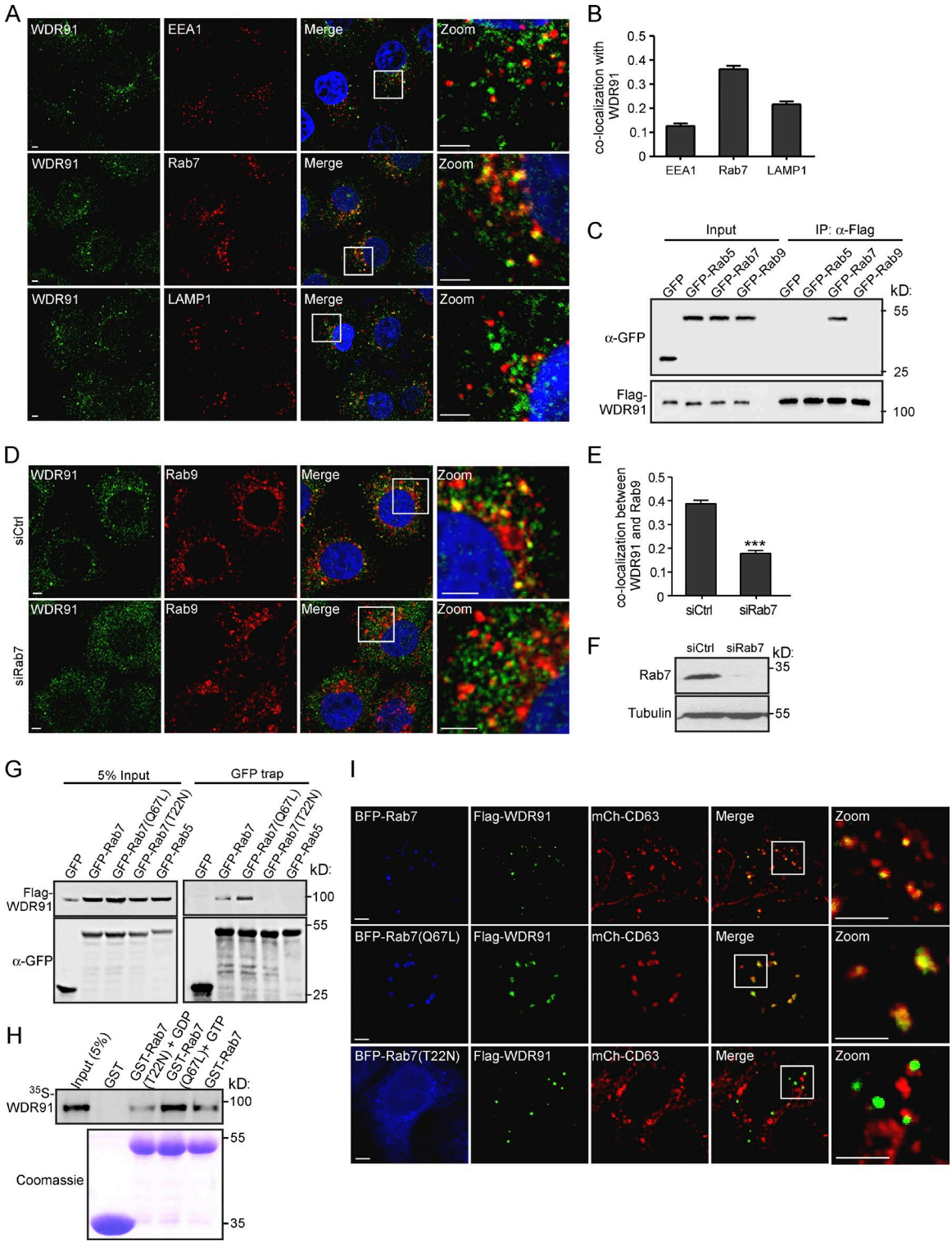

Figure 3. **WDR91 is recruited to endosomes by interacting with GTP-Rab7.** (A) Coimmunostaining of endogenous WDR91 with EEA1, Rab7, LAMP1, and Sec61-β in HeLa cells. (B) Quantification of the colocalization as shown in A. (C) Co-IP of Flag-WDR91 with GFP-tagged Rab7, Rab5, and Rab9. IPs were performed with Flag antibody, and precipitated proteins were detected with antibodies to Flag or GFP. (D and E) Colocalization (D) and quantification (E) of endogenous WDR91 with Rab9 in cells treated with siCtrl and Rab7 siRNA (siRab7). (F) Immunoblotting of Rab7 in HeLa cells treated with siCtrl or siRab7. (G) Co-IP of GFP-tagged Rab7, Rab7(Q67L), and Rab7(T22N) with Flag-WDR91. IPs were performed with GFP-trap beads, and precipitated proteins were detected with Flag antibody. (H) Purified GST, GST-Rab7, GST-Rab7(Q67L), and GST-Rab7(T22N) were first incubated with GTP or GDP as indicated, immobilized on glutathione–Sepharose beads and then incubated with ^{35}S-labeled WDR91 prepared by in vitro translation. After extensive washing, bound proteins were resolved by SDS-PAGE and viewed with autoradiography. (I) Colocalization of Flag-WDR91 with mCh-CD63 in HeLa cells coexpressing BFP-Rab7, BFP-Rab7(Q67L), and BFP-Rab7(T22N). Zoom images represent magnified views of boxed areas. Bars, 5 µm. On graphs showing quantification of protein colocalization (B and E), Pearson's correlation coefficient is plotted on the y-axis. ≥50 cells were scored. Error bars represent SEM. ***, $P < 0.001$.

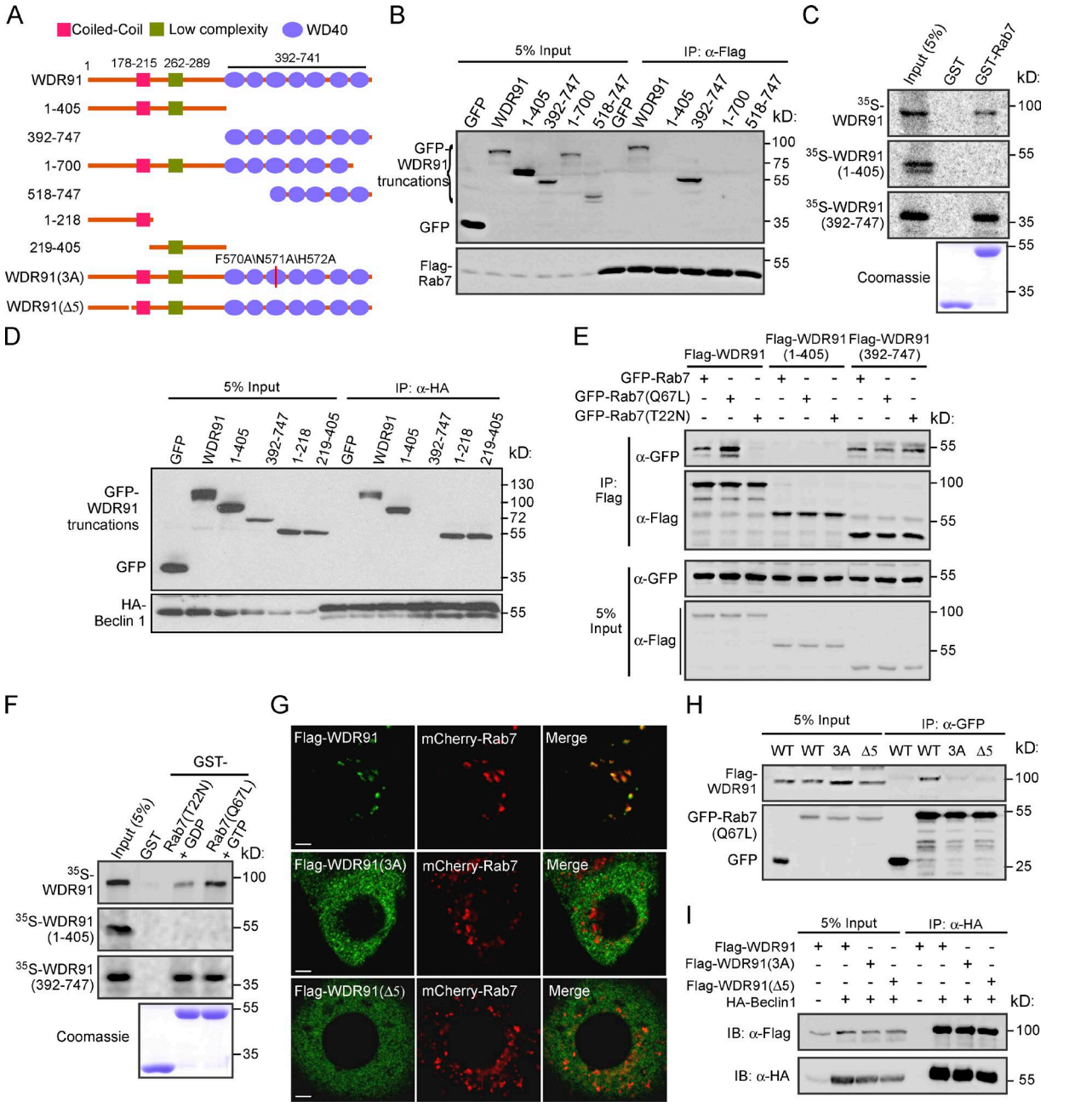

Figure 4. **Characterization of the interaction of WDR91 with Rab7.** (A) Schematic depiction of WDR91 truncations and mutants. (B) Co-IP of Flag-Rab7 with GFP-tagged WDR91 truncations. IPs were performed with Flag antibody, and precipitated proteins were detected with antibodies to Flag and GFP. (C) Purified GST and GST-Rab7 were immobilized on glutathione–Sepharose beads and incubated with ^{35}S-labeled WDR91 proteins prepared by in vitro translation. After extensive washing, bound proteins were resolved by SDS-PAGE and viewed with autoradiography. (D) Co-IP of HA-Beclin1 with GFP-tagged WDR91 truncations. IPs were performed with Flag antibody, and precipitated proteins were detected with antibodies to HA and GFP. (E) Co-IP of Flag-tagged WDR91, WDR91(1–405), and WDR91(392–747) with GFP-tagged Rab7(WT), Rab7(Q67L), and Rab7(T22N). IPs were performed with Flag antibody, and precipitated proteins were detected with antibodies to Flag and GFP. (F) Purified GST, GST-Rab7(Q67L), and GST-Rab7(T22N) immobilized on glutathione–Sepharose beads were incubated with GTP or GDP as indicated and then incubated with ^{35}S-labeled WDR91 proteins prepared by in vitro translation. After extensive washing, bound proteins were resolved by SDS-PAGE and viewed with autoradiography. (G) Confocal images of the colocalization of Flag-WDR91, Flag-WDR91(3A), or Flag-WDR91(Δ5) with mCh-Rab7. Bars, 5 µm. (H) Co-IP of GFP-Rab7(Q67L) with Flag-tagged WDR91(WT), WDR91(3A), and WDR91(Δ5). IPs were performed with GFP-trap beads, and precipitated proteins were detected with the indicated antibodies. (I) Co-IP of HA-Beclin1 with Flag-tagged WDR91(WT), WDR91(3A), and WDR91(Δ5). IPs were performed with HA antibody, and precipitated proteins were detected with antibodies to HA and Flag.

S4 E). The expression of WDR91 was effectively inactivated in the brain of *Wdr91* cKO mice (Fig. S4 F). *Wdr91* cKO mice were viable and indistinguishable from the control littermates at birth. However, *Wdr91* cKO mice displayed progressive growth retardation and smaller brain size during postnatal development (Fig. 6, A–C) and succumbed to death at ∼4 wk of age (Fig. 6 D). Histological analyses of brain sections revealed an obvious reduction in cortex thickness in *Wdr91* cKO mice compared with the WT (Fig. S4, G and H). We next examined the cytoarchitecture of neurons by performing Golgi staining. *Wdr91* cKO mice

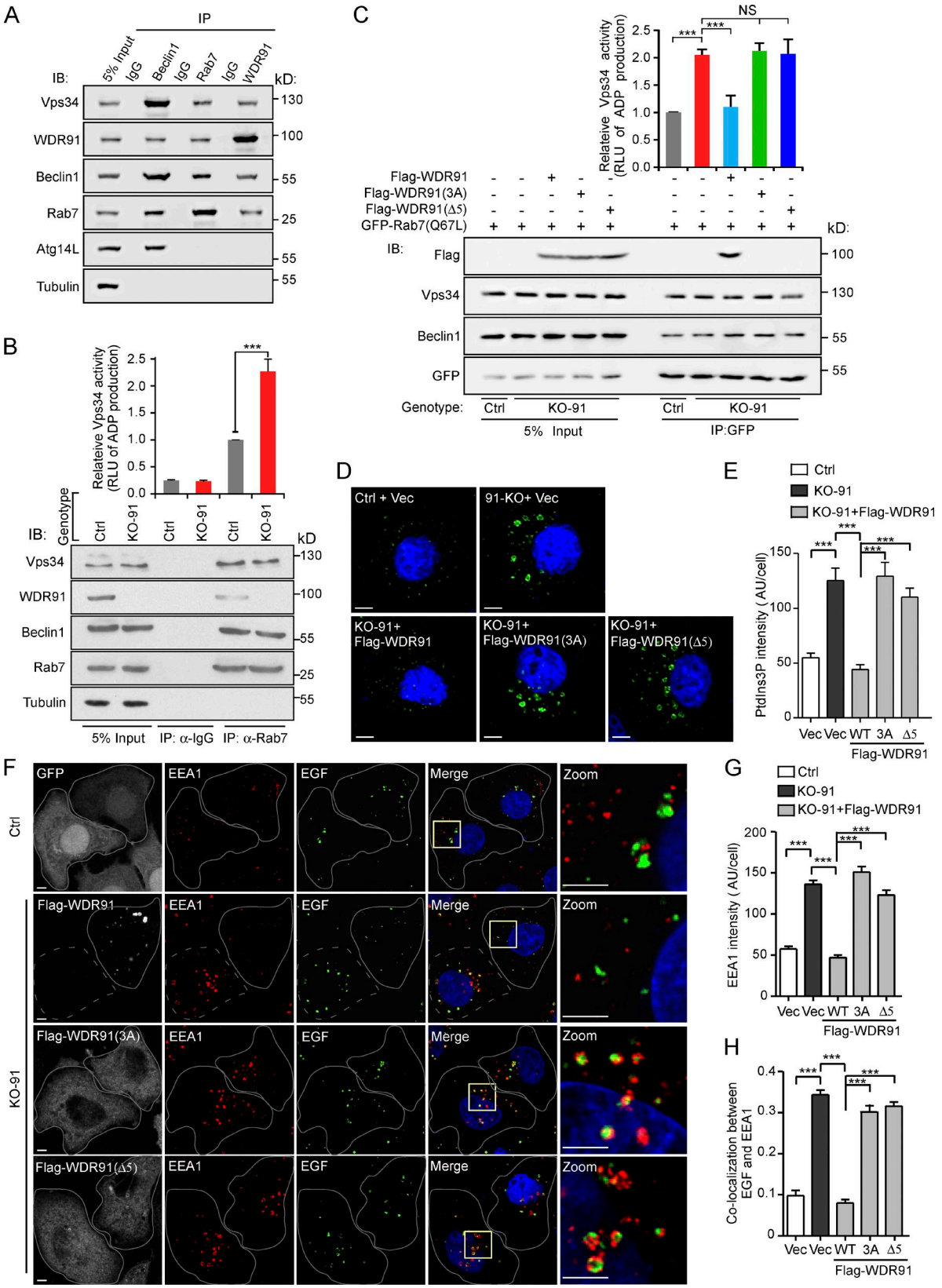

Figure 5. **WDR91 interacts with and inhibits the activity of the Rab7-associated PI3K complex.** (A) IP of endogenous Beclin1, Rab7, and WDR91 from HeLa cells using their cognate antibodies. Coprecipitated proteins were detected with antibodies against the indicated proteins. (B) Loss of WDR91 enhances the activity of the Rab7-associated PI3K complex. Endogenous Rab7 was immunoprecipitated from cell lysates of Ctrl and KO-91 HeLa cells. Precipitated proteins were detected with antibodies to the indicated proteins (bottom). Equal amounts of precipitated Vps34 from each genotype were examined for PI3K activity by measuring the relative units of luminescence (RLU) of ADP converted from ATP. (C) Rescuing effects of Flag-tagged WDR91(WT), WDR91(3A), and WDR91(Δ5) on the activity of the Rab7-associated PI3K complex in KO-91 cells. Control and KO-91 HeLa cells were cotransfected with

exhibited a marked reduction in neuronal arborization in both the hippocampal dentate gyrus and the cortex (Fig. 6 E and Fig. S5 A). Further quantification confirmed that ablation of *Wdr91* led to a significant reduction in dendritic length and complexity of granular neurons during postnatal hippocampal development (Fig. 6, F and G). In addition, a strong increase in Caspase 3 activation was detected in *Wdr91* cKO mouse brains (Fig. S5 B), suggesting that *Wdr91* inactivation caused excessive apoptosis of neurons. Together, these data indicate that brain-specific inactivation *Wdr91* caused developmental defects of neurons and consequently of the brain in mice.

WDR91 maintains endosome conversion required for neuronal development

To determine whether WDR91 promotes neuronal development by acting in the endosome–lysosome pathway, we examined endosomes in hippocampal neurons isolated from *Wdr91* KO mice. Compared with WT cells, *Wdr91*$^{-/-}$ neurons contained a very high percentage of greatly enlarged intermediate endosomes that were positive for both EEA1 and mCh-Rab7 in cell bodies and dendrites (Fig. 7 A and Fig. S5 C). This suggests that WDR91 is required for early-to-late endosome conversion in mouse neurons, like in human cells. Importantly, reintroducing Flag-WDR91, which localized to Rab7-positive but not 2×FYVE-positive endosomes in neurons (Fig. S5 D), successfully rescued the formation of enlarged intermediate endosomes in *Wdr91*$^{-/-}$ neurons (Fig. 7 B). In contrast, expression of Flag-WDR91(3A) or Flag-WDR91(Δ5) did not have similar rescuing effects (Fig. 7 B). Given that WDR91(3A) and WDR91(Δ5) do not interact with Rab7, WDR91 probably fulfills its role in endosome conversion in a manner that depends on its interaction with Rab7 in neuronal cells. In addition, *Wdr91*$^{-/-}$ hippocampal neurons cultured in vitro showed strongly reduced dendritic length and complexity compared with WT neurons (Fig. 7, C–E). The shortened length and reduced arborization of *Wdr91*$^{-/-}$ neurons were mostly rescued by reexpressing WT WDR91 but not the Rab7 binding-deficient WDR91(3A) or WDR91(Δ5) mutants (Fig. 7, C–E). Collectively, these results suggest that WDR91 is required for neuronal development by acting as a Rab7 effector to maintain appropriate early-to-late endosome conversion.

Discussion

In this study, we demonstrated that WDR91 is a novel Rab7 effector that couples Rab switching with inhibition of endosomal PtdIns3P generation for early-to-late endosome conversion in the endosome–lysosome pathway. Our findings indicate that endosomal recruitment of WDR91 depends on the active GTP-Rab7. The C and N termini of WDR91 simultaneously interacted with GTP-Rab7 and Beclin1. Loss of WDR91 led to endosomal accumulation of PtdIns3P and formation of greatly enlarged intermediate endosomes, thus preventing the delivery of endosomal cargoes to the lysosome. Importantly, the increased activity of the Rab7-associated PI3K complex in *Wdr91* KO cells was rescued by WT WDR91 but not WDR91 mutants that were unable to interact with Rab7. Consistent with this, WT WDR91, but not Rab7 binding-deficient mutants, rescued the defective endosome–lysosome trafficking in *WDR91* KO HeLa cells. In addition, our findings revealed the essential role of WDR91 in neuronal development. Though global deletion of *Wdr91* caused neonatal death, brain-specific KO of *Wdr91* led to an obvious reduction in brain size and a thinner cerebral cortex in mice. Like KO-91 HeLa cells, *Wdr91*-deficient mouse neurons accumulated giant intermediate endosomes in both cell bodies and neurites, and the dendritic development was severely impaired. Moreover, the neuronal function of WDR91 required the interaction with Rab7, providing further evidence that WDR91 functions as an important Rab7 effector that is essential for endosome–lysosome trafficking and hence neuronal development.

Our findings suggest that coordination of Rab switching and PtdIns3P down-regulation is required for early-to-late endosome conversion. The active GTP-Rab5 recruits the PI3K complex to early endosomes to facilitate the synthesis of endosomal PtdIns3P, which acts through effectors to drive early endosome fusion and maturation, cargo sorting, and other early endosomal events (Christoforidis et al., 1999; Lindmo and Stenmark, 2006; Schink et al., 2013). It is thus conceivable that Mon1/SAND-1–mediated replacement of Rab5 with Rab7 can terminate the positive effect of Rab5 on the PI3K complex. Nevertheless, Rab7 also interacts with the PI3K complex, but PtdIns3P levels are much lower on late endosomes than on early endosomes (Gillooly et al., 2000; Stein et al., 2003). Our findings now demonstrate that the activity of the Rab7-associated PI3K complex is suppressed by the Rab7 effector WDR91. Upon endosomal activation of Rab7, the active GTP-Rab7 recruits WDR91 to the endosome, where it also interacts with the PI3K complex and inhibits the synthesis of PtdIns3P. In the meantime, the existing PtdIns3P on late endosomes can be dephosphorylated by myotubularin phosphatases or converted into PtdIns(3,5)P_2 by PIKfyve/Fab1 (Wurmser and Emr, 1998; Dove et al., 2009; Hnia et al., 2012; Schink et al., 2013). In addition, it is possible that PtdIns3P is invaginated into the endosomal lumen for degradation (Stenmark and Gillooly, 2001). This WDR91-mediated coordination of Rab5-to-Rab7 switching and PtdIns3P down-regulation enables the conversion of early endosomes to late endosomes and hence the delivery of endosomal cargoes to the lysosome.

Several lines of evidence suggest that Rab7 plays an important role in early endosomal trafficking. For example, constitutive expression of dominant-negative Rab7 traps

vectors expressing GFP-Rab7(Q67L) and the indicated WDR91 proteins. 36 h later, cell lysates were subjected to IP using GFP-trap beads. Precipitates were detected with antibodies against the indicated proteins (bottom) and analyzed for PI3K activity as in B. (B and C) Data representing mean ± SEM are from three independent experiments and are normalized to PI3K activity in Ctrl cells (top). (D and E) Immunostaining (D) and quantification (E) of PtdIns3P levels in control and KO-91 HeLa cells transfected with the indicated vectors expressing Flag-WDR91, Flag-WDR91(3A), and Flag-WDR91(Δ5) for 24 h. Bars, 5 µm. (F) Rescuing effects of Flag-WDR91, Flag-WDR91(3A), and Flag-WDR91(Δ5) on defective endosomal EGFR trafficking in KO-91 cells. Control or KO-91 HeLa cells were transfected with vectors expressing the indicated Flag-WDR91 proteins for 24 h and were stimulated with 2 µg/ml Alexa Fluor 647–conjugated EGF. 60 min after stimulation, cells were fixed and stained with EEA1 and Flag antibodies. Solid lines mark the cells expressing the indicated proteins. Dashed lines mark cells that do not express WT or mutant WDR91. Zoom images represent magnified views of boxed areas. Bars, 5 µm. (G and H) Quantification of the intensity of EEA1 staining (G) and the colocalization of EEA1 with EGFR (H) as shown in F. Data represent mean ± SEM in G and Pearson's correlation coefficient in H. ≥50 cells were scored. ***, $P < 0.001$.

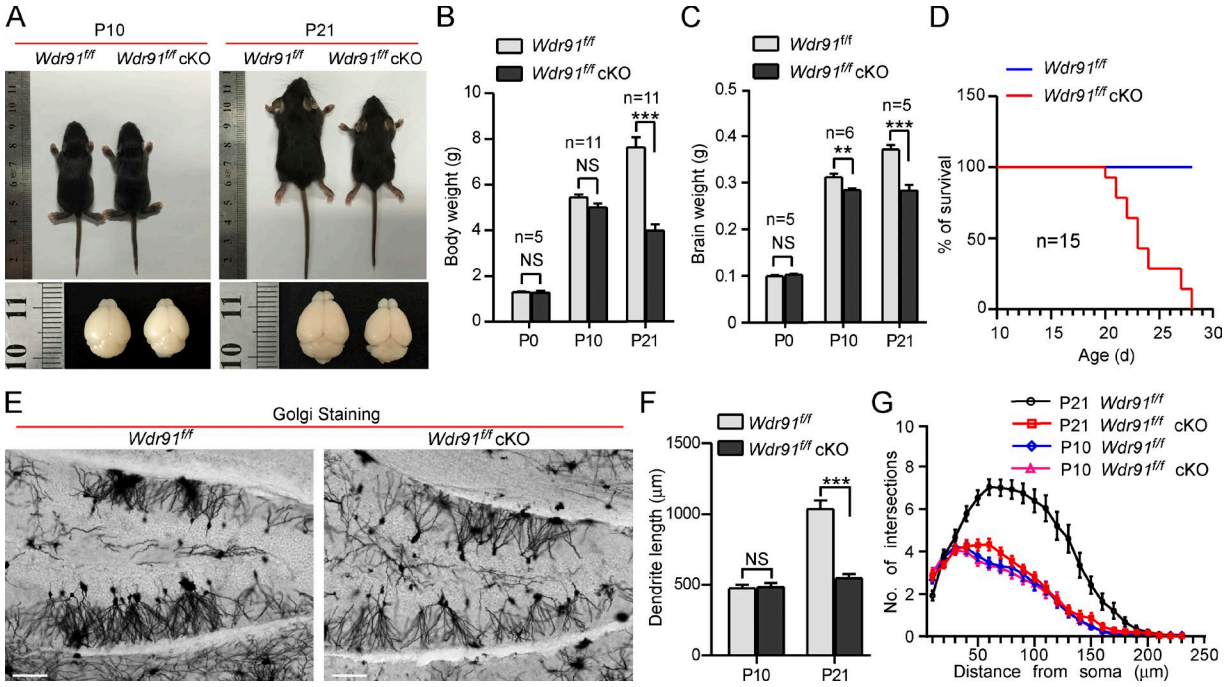

Figure 6. **WDR91 is important for postnatal development in mice.** (A) Representative images of *Wdr91*$^{f/f}$ and *Wdr91*$^{f/f}$ cKO mice and their brains at postnatal day 10 (P10) and P21. (B) Body weight of *Wdr91*$^{f/f}$ and *Wdr91*$^{f/f}$ cKO mice at P0, P10, and P21. (C) Brain weight of *Wdr91*$^{f/f}$ and *Wdr91*$^{f/f}$ cKO mice at P0, P10, and P21. (D) Survival curve of postnatal *Wdr91*$^{f/f}$ and *Wdr91*$^{f/f}$ cKO mice. (E) Representative images of the granular neurons in the hippocampus of *Wdr91*$^{f/f}$ and *Wdr91*$^{f/f}$ cKO mice at P21. Neurites and cell bodies were revealed by Golgi staining of the brain sections. Bars, 100 µm. (F) Quantification of the cumulative length of the dendritic processes of the hippocampal neurons in *Wdr91*$^{f/f}$ and *Wdr91*$^{f/f}$ cKO mice at P10 and P21. (G) Quantification of the dendritic branches of the hippocampal neurons in *Wdr91*$^{f/f}$ and *Wdr91*$^{f/f}$ cKO mice at P10 and P21 with Sholl analysis. (F and G) ≥30 neurons from three mouse brains were scored. For all quantifications, error bars represent SEM. *n* indicates the number of mice analyzed. **, P < 0.01; ***, P < 0.001.

vesicular stomatitis virus G protein and CI-MPR (cation-independent mannose 6-phosphate receptor) in early endocytic compartments (Press et al., 1998; Vonderheit and Helenius, 2005). siRNA knockdown of Rab7 leads to accumulation of low-density lipoproteins, CI-MPR, and IFN-α chain 1 (IFN AR1) in enlarged EEA1-positive early endosomes (Girard et al., 2014). These trafficking defects caused by Rab7 inactivation are quite similar to those resulting from loss of WDR91. The identification of WDR91 as a Rab7 effector therefore provides a mechanistic explanation for the requirement for Rab7 in early endosomal trafficking. Inactivation of Rab7 leads to a failure to recruit WDR91 to endosomes, which in turn causes an elevation in endosomal PtdIns3P levels and consequently trapping of endosomal cargoes in the enlarged intermediate endosomes as seen in KO-91 cells. This also suggests that WDR91 is an essential effector for Rab7 to promote movement of cargo out of the endosomes.

Endosomal trafficking plays important roles in neuron survival and neurite outgrowth (Tang, 2008; Yap and Winckler, 2012). Several Rab7 mutations have been found to be associated with Charcot-Marie-Tooth type 2B (CMT2B) neuropathies, which manifest as neuron degeneration with loss of nerve fibers. Although these mutations likely lead to a high proportion of active GTP-Rab7 (Spinosa et al., 2008; BasuRay et al., 2010), knockdown of Rab7 was also shown to impede the final phase of neuronal migration and induce abnormal dendrite morphology (Kawauchi et al., 2010). Our findings indicate that, as a Rab7 effector, WDR91 is required for normal mouse brain development. Neuron-specific KO of *Wdr91* leads to reduced brain volume and thinning of the cerebral cortex. These defects might result from reduction in neurite complexity and elevated apoptosis in the *Wdr91* cKO mouse brain. At the cellular level, *Wdr91*-deficient neurons accumulate giant intermediate endosomes with diameters even as large as that of dendrites. These huge endosomes may disturb signal transduction and/or vesicular transport through the dendrites, thus impairing dendritic outgrowth (Barford et al., 2017). Future studies will be needed to investigate how WDR91-mediated endo-lysosomal trafficking affects the signaling events required for neuronal development. In addition, further investigation will reveal how WDR91 coordinates with other Rab7 effectors, such as RILP, FYCO, ORPL1, Protrudin, EPG5, and PLEKHM1 (Johansson et al., 2007; Pankiv et al., 2010; McEwan et al., 2015; Raiborg et al., 2015; Wang et al., 2016), to regulate Rab7-dependent cellular processes. In particular, it will be of great interest to explore the cell- or tissue-specific requirement for WDR91 in development and to investigate whether WDR91 mutations are associated with human neurological disorders as well as other diseases.

Materials and methods

Antibodies, reagents, and expression vectors

EEA1 mouse monoclonal antibody was purchased from BD Biosciences. EEA1, Rab7, Rab9, Vps34, Beclin1, Lamp1, and activated caspase 3 rabbit monoclonal antibodies were purchased from Cell Signaling Technologies. EGFR and SEC61β rabbit polyclonal antibodies, p230 and NeuN mouse monoclonal antibodies, and LacZ chicken polyclonal antibody were purchased from Abcam. Beclin1 rabbit polyclonal antibody was purchased from Medical & Biological Laboratories. PtdIns3P

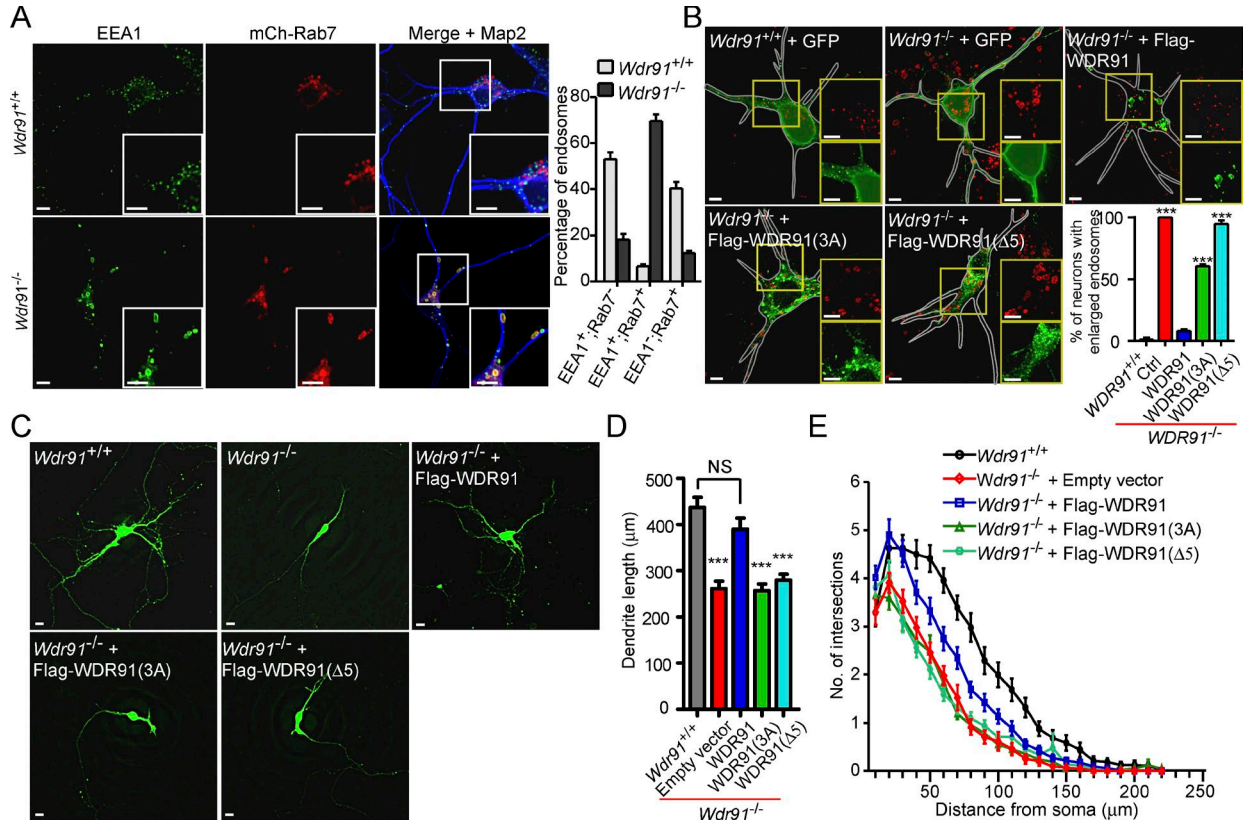

Figure 7. **WDR91 is required for endosome conversion in mouse neurons.** (A) Endosome conversion is compromised in neuronal cells of *Wdr91*$^{-/-}$ mice. Immunostaining of EEA1, mCh-Rab7, and Map2 in cultured primary hippocampal neurons isolated from *Wdr91*$^{+/+}$ and *Wdr91*$^{-/-}$ mice (left). Neurons were transfected with vectors expressing mCh-Rab7 at the fourth day after isolation and subjected to immunostaining 3 d after transfection. Quantification of endosomes that were positive for EEA1 and negative for Rab7 (EEA1^{+};Rab7^{-}), positive for both EEA1 and Rab7 (EEA1^{+};Rab7^{+}), and positive for Rab7 and negative for EEA1 (EEA1^{-};Rab7^{+}) in cultured primary hippocampal neurons (right). ≥10 neurons were scored. Data representing means ± SEM are from three independent experiments. (B) Rescuing effects of Flag-WDR91, Flag-WDR91(3A), and Flag-WDR91(Δ5) on EEA1-positive endosomes in the primary hippocampal neurons isolated from *Wdr91*$^{-/-}$ mice. Neurons isolated from *Wdr91*$^{+/+}$ or *Wdr91*$^{-/-}$ mice were transfected with vectors expressing the indicated proteins and then subjected to immunostaining of EEA1 (red) and GFP or Flag (green) 3 d after transfection. Insets show magnified images of the boxes in the merged images. Quantification of neurons with giant endosomes after transfection is shown at the bottom right. ≥25 neurons were scored. Data representing means ± SEM are from three independent experiments. (C) Representative images of primary hippocampal neurons isolated from *Wdr91*$^{+/+}$ or *Wdr91*$^{-/-}$ mice. Neurons with the indicated genotype were transfected with a GFP-expressing vector and individual vectors expressing the indicated WDR91 proteins. (D) Quantification of the cumulative length of the dendrites of hippocampal neurons shown in C. ≥35 neurons were scored. (E) Quantification by Sholl analysis of the dendritic branches of hippocampal neurons shown in C. ≥30 neurons were scored. Data represent means ± SEM in all quantifications. ***, $P < 0.001$. Bars, 20 µm.

mouse monoclonal antibody was purchased from Echelon Biosciences. Map2, CI-MPR, Flag, and Myc mouse monoclonal antibodies and GST rabbit polyclonal antibody were purchased from Sigma-Aldrich. S100-β rabbit polyclonal antibody was purchased from Dako. WDR91 antibody was generated in mice by GST-WDR91(406–730) injection. Rab7 mouse polyclonal antibody was generated in mice by GST-Rab7 injection. GFP antibody was generated in mice and rabbits by purified His-GFP injection. Alexa Fluor dye–conjugated secondary antibodies were purchased from Life Technologies.

Dextran blue (405) and dextran Alexa Fluor 488 (molecular weight, 10,000), Alexa Fluor 647–conjugated EGF, and LysoTracker red DND-99 were purchased from Life Technologies. ADP-GloTM kinase assay kit was purchased from Promega. FD Rapid Golgi staining kit was purchased from FD Neurotechnologies.

Bacterial and mammalian expression vectors were constructed using standard protocols and are listed in Table S1.

Cell culture and small RNA interference

HeLa or HEK293 cells were cultured at 37°C with 5% CO_2 in DMEM supplemented with 10% FBS (HyClone), 100 U/ml penicillin, and 100 mg/ml streptomycin.

Transfections were performed with Lipofectamine 2000 (Invitrogen) according to the manufacturer's instructions.

siRNA was achieved by transfection of the following oligos: Rab7, 5′-GAACACACGUAGGCCUUCATT-3′ (Spinosa et al., 2008); Beclin1, 5′-CAGUUUGGCACAAUCAAUA-3′ (Zhong et al., 2009); and control, 5′-UUCUCCGAACGUGUCACGUTT-3′. Cells were harvested for Western blot or observed by microscopy 24 h after transfection.

Isolation, culture, and transfection of primary hippocampal neurons

Hippocampal neurons were isolated from *WDR91*$^{+/+}$ or *WDR91*$^{-/-}$ P0 mice. In brief, hippocampi were microdissected in ice-cold HBSS (Gibco) and incubated in 0.05% trypsin-EDTA (Invitrogen) for 15 min at RT. The dispersed hippocampal neurons were cultured at 37°C with 5% CO_2 in neurobasal medium (Invitrogen) supplemented with 2% B27, 0.5 mM L-glutamine, and 1% antibiotics.

Hippocampal neurons were transfected 4 d after isolation as they were actively undergoing dendritic morphogenesis. 1 µg of total DNA and 1 µl of Lipofectamine 2000 reagent that was diluted in OptiMEM medium (Gibco; Invitrogen) were used per well in a 24-well plate. The neurons were fixed for morphological analysis 72 h after transfection.

Expression vectors

pmCherry-CD63 was provided by H. Zhang (Institute of Biophysics, Chinese Academy of Sciences, Beijing, China). pCMV-HA-Beclin1 was provided by X. Wang (Institute of Biophysics, Chinese Academy of Sciences). Bacterial and mammalian cell expression vectors are listed in Table S1.

Endosomal trafficking assays

For EGFR trafficking assays, cells were grown on coverslips and treated with 25 ng/ml EGF or 2 µg/ml Alexa Fluor 647–conjugated EGF for 10 min. Cells were washed twice with DMEM and fixed at indicated time points for further analysis.

Immunostaining

For staining with most of the primary antibodies, HeLa cells or cultured hippocampus neurons grown on coverslips were fixed in 4% paraformaldehyde followed by permeabilization with 0.2% saponin for 8 min. For staining with the Rab7 and WDR91 antibodies, cells grown on coverslips were fixed in 4% paraformaldehyde and permeabilized with 0.3% Triton X-100 for 15 min. After extensive washing with PBS, coverslips were incubated in blocking buffer (5% BSA, 0.05% saponin, and PBS) for 1 h at RT and then incubated with primary antibodies in blocking buffer at 4°C overnight. Cells were washed extensively again and incubated with Cy3- or FITC-conjugated secondary antibodies in blocking buffer for 1 h at RT. After another round of extensive washing, cells were sealed with VECTASHIELD mounting medium (Vector Laboratories) for confocal microscopy analysis.

For immunostaining of endosomal PtdIns3P, a detergent-free method was used as described previously (Liu et al., 2016). In brief, cells grown on coverslips were washed twice with ice-cold glutamate buffer (25 mM Hepes, pH 7.4, 25 mM KCl, 2.5 mM Mg-acetate, 5 mM EGTA, and 150 mM K-glutamate) and then frozen in liquid N_2 thoroughly. After thaw, cells were washed twice with ice-cold glutamate buffer again. Cells were then fixed with 3.7% (wt/vol) formaldehyde in 200 mM Hepes, pH 7.4, for 30 min at RT, followed by washing twice with blocking buffer 2 (1% BSA in PBS; 10 min for each) and subsequently incubating in blocking buffer 2 for an additional 30 min. The cells were then incubated with 5 µg/ml PtdIns3P antibody blocking buffer 2 at 4°C overnight. Cells were washed extensively again with blocking buffer 2 and incubated with FITC-conjugated secondary antibody for 1 h at RT. After another round of thorough washing, coverslips were washed once more with double-distilled H_2O and mounted with VECTASHIELD mounting medium for confocal microscopy analysis.

Microscopy

For fixed cells, fluorescent images were obtained with an inverted confocal microscope system (FV1000; IX81; Olympus) coupled with a camera (FV10-SPD; Olympus) using a 60× 1.42 NA oil objective. Excitation was achieved using solid-state 488-nm and gas-state 595-nm lasers in confocal microscopy analysis. All images were taken at RT and processed with viewer software (FV10-ASW 4.0a; Olympus). For measurement of intensity and colocalization, a line was drawn along the boundary of the cell to fully surround the cell. Then, the integrated intensity of each channel of interest and the Pearson's correlation coefficient between the channels of interest were determined with the same software.

To record the dynamics of endosomes in HeLa cells, images were obtained with the DeltaVision imaging system (DV ELITE; GE Healthcare) coupled with a camera (CoolSNAP; Photometric Scientific) using a 100× 1.40 NA oil objective. Cells were plated in glass-bottom dishes (MatTek) in DMEM supplemented with 10% FBS. During imaging, the glass-bottom dishes were placed in a humidified chamber (Clamlide TC) supplemented with 5% CO_2 at 37°C. Images were captured every 30 s for 60 min with a Z series of 0.4 µm/section for a total of 15 sections. After acquisition, the images were deconvoluted with the Enhanced Ratio option. Five images containing interested organelles were projected to form one image by maximum-intensity projection using softWoRx software (GE Healthcare). The excitation filters used for GFP and mCherry in all images were 488 and 559 nm, respectively.

Recombinant proteins and GST pull-down

Recombinant GST-Rab7, GST-Rab7(T22N), and GST-Rab7(Q67L) proteins were expressed in BL21(DE3) bacterial cells and purified with glutathione–Sepharose beads (Amersham) according to the instructions provided by the supplier. ^{35}S-labeled WDR91, WDR91(1–405), and WDR91(392–747) proteins were prepared by in vitro translation. Purified GST-tagged proteins (2.5 µg of each) were immobilized on glutathione–Sepharose beads and incubated with ^{35}S-labeled WDR91, WDR91(1–405), or WDR91(406–747) in binding buffer (50 mM Tris-HCl, pH 8.8, 150 mM NaCl, 5 mM MgCl, 10 mM DTT, 0.05% NP-40, 1 mM PMSF, and protease inhibitor cocktail) at 4°C for 2 h. To examine the interactions of WDR91 with constitutively active (GTP) or dominant-negative (GDP) forms of Rab7, GST-Rab7 proteins immobilized on glutathione–Sepharose beads were first incubated in binding buffer supplemented with 10 mM GTP or 10 mM GDP at 37°C for 1 h and then incubated with ^{35}S-labeled WDR91, WDR91(1–405), or WDR91(406–747) at 4°C for 2 h in binding buffer supplemented with 10 mM GTP or GDP. After extensive washing with binding buffer, bound proteins were resolved on SDS-PAGE and visualized by autoradiography.

IP and GFP-trap pull-down

For the IP of endogenous proteins, cells were lysed in lysis buffer 1 (20 mM Tris-HCl, pH 7.5, 150 mM NaCl, 10 mM MgCl, 1% Triton X-100, and protease inhibitor cocktail). The IPs were performed as described previously using individual antibodies (Chen et al., 2013). For GFP-trap pull-down, cells expressing GFP-tagged proteins were lysed in the same lysis buffer and then the cell lysates were incubated with GFP-trap beads (ChromoTek) for 1 h at 4°C. After extensive washing with the cell lysis buffer, the precipitated proteins were resolved by SDS-PAGE and detected by Western blotting with relevant antibodies.

In vitro PI3K complex activity assay

HeLa cells of different genotypes or transfected with the indicated vectors for 24 h were harvested and lysed in lysis buffer 2 (50 mM Tris-HCl, pH 7.4, 10 mM MgCl, 150 mM NaCl, 1% Triton X-100, and protease inhibitor cocktail). Endogenous PI3K complex and WDR91 were immunoprecipitated with Rab7 antibody using protein A beads. In PI3K activity rescuing assays, the cells that coexpressed GFP-Rab7(Q67L) with different Flag-WDR91 mutant forms were lysed with lysis buffer 2 and incubated with GFP-Trap beads overnight at 4°C. The GFP-Trap beads with precipitated GFP-Rab7, Flag-WDR91, Vps34, and Beclin1 were extensively washed with lysis buffer 2 and further washed twice with reaction buffer (40 mM Tris-HCl, pH 7.5, 10 mM $MgCl_2$, and 1 mg/ml BSA). The beads were then incubated with 10 µg sonicated phosphatidylinositol (Sigma-Aldrich) and 1 µl ATP (10 mM) in 30 µl of reaction buffer with continuous shaking for 30 min at RT. Conversion of ATP to ADP was measured with an ADP-GloTM kinase assay kit according to the instructions provided by the manufacturer.

Quantitative real-time PCR

Total RNA was isolated from different organs of a C57B/L6 male mouse using TRIzol Reagent (Invitrogen) according to the manufacturer's instructions. Reverse transcription of mRNA was performed with a reverse transcription kit (Promega) in a 20-µl reaction mixture. WDR91 expression was examined in triplicate using a real-time PCR system

(7900HT Fast; Applied Biosystems). Endogenous GAPDH was amplified as the internal control.

Generation of *Wdr91* KO mice

Wdr91$^{-/-}$ mice and *Wdr91*$^{f/f}$ mice were generated by BIOCYTOGEN. *WDR91*$^{f/f}$ and *Nestin-Cre* mice were bred onto the C57B/L6 background and housed at the animal facility at the Institute of Genetics and Developmental Biology (IGDB), Chinese Academy of Sciences. All procedures and husbandry were performed according to protocols approved by the Institutional Animal Care and Use Committee at IGDB.

Immunohistology

Mice were anesthetized and trans-cardially perfused with saline followed by 4% paraformaldehyde. The brains were dissected out and postfixed in 4% paraformaldehyde for 24 h. For hematoxylin-eosin staining, the brains were subjected to paraffin-embedded sectioning. In brief, the brains were dehydrated sequentially in graded ethanols (70, 80, and 95% for 1 h each, followed by 100% ethanol for 1 h, three times) and then the ethanol was cleared in xylene for 1 h with two repeats. The brains were immersed in paraffin for 1 h with three repeats and then sectioned at 8 µm on a microtome. The sections were deparaffinized in xylene for 10 min with three repeats and rehydrated by sequential incubation in graded ethanols (100, 100, 95, 80, 70, and 50%, each for 5 min). The sections were stained with 1× hematoxylin for 18 min, washed with distilled water for 3 s and acid alcohol for 2 s and then rinsed with distilled water for 14 min. After poststaining with 0.5% eosin for 70 s, the sections were washed with 100% ethanol for 2 min with three repeats and xylene for 2 min with three repeats and finally mounted for microscopy analysis.

For immunofluorescence staining, the brains were subjected to cryosectioning. In brief, the fixed brains were dehydrated in 30% sucrose for at least 48 h and frozen in 30% sucrose. Brain sections (40-µm thickness) were generated using a sliding microtome equipped with a −20°C freezer and transferred into 96-well plates filled with cryoprotectant solution (glycerol, ethylene glycol, and 0.1 M phosphate buffer, pH 7.4, 1:1:2 by volume). After extensive washing with PBS, the sections were incubated in blocking buffer (5% donkey serum, 0.25% Triton X-100, and PBS) for 1 h at RT and then incubated with primary antibodies in blocking buffer at 4°C overnight. Then, the sections were washed extensively again and incubated with Alexa Fluor 488–, 568–, or 647–conjugated secondary antibodies in blocking buffer for 2 h at RT. The sections were mounted, coverslipped, and maintained at 4°C in the dark until analysis.

Golgi staining

Golgi staining was performed according to the manufacturers' instructions (FD Neurotechnologies). Pictures were captured using a microscope (Axioimager M1; Zeiss; 10× NA 0.3) coupled with a monochrome digital camera (AxioCam) and Axiovision rel. 4.7 software.

Neurite complexity analysis

Cultured neurons were imaged with a microscope (Axioimager M1; 20× NA 0.5) coupled with a monochrome digital camera (AxioCam). For measurement of dendrite length and neurite intersections, images were analyzed by ImageJ analysis software (National Institutes of Health) using the neurite tracing and Sholl analysis plug-ins, respectively. 30 neurons from three animals per genotype were subjected to analysis.

Protein structure prediction

Molecular modeling of the WD40-repeat domain of WDR91 was obtained using the Phyre2 Protein Homology Recognition Engine (template PDB accession no. 3DM0; http://www.sbg.bio.ic.ac.uk/phyre2/html/). The pictures were generated using PyMOL (The PyMOL Molecular Graphics System, version 1.7.4; Schrödinger). Docking analysis was performed with the GRAMM-X web server using the Rab7 structure and WDR91 WD40-repeat homology model.

Statistical analysis

The statistical analyses were performed using Prism (GraphPad Software) or Excel (Microsoft Office) to generate curves or bar graphs. All error bars represent SEM. The two-tailed unpaired *t* test was used for statistical analysis of two groups of samples. One-way ANOVA with a Newman-Keuls posttest was used to evaluate the statistical significance of multiple groups of samples. *, $P < 0.05$; **, $P < 0.01$; ***, $P < 0.001$. $P > 0.05$ was considered NS.

Online supplemental material

Fig. S1 characterizes the intermediate endosomes in KO-91 cells and the requirement of Rab7 for endosomal association of WDR91. Fig. S2 identifies amino acid residues required for WDR91–Rab7 interaction. Fig. S3 shows the rescuing effects of WT and mutant WDR91 on endosomal trafficking of dextran in KO-91 cells. Fig. S4 shows that *Wdr91* KO impairs mouse development. Fig. S5 describes that *Wdr91* inactivation in the brain causes defective neuronal development. Videos 1 and 2 show time-lapse monitoring of early-to-late endosome conversion. Table S1 lists expression constructs and is included as an Excel file.

Acknowledgments

We thank Dr. I. Hanson for proofreading the manuscript.

W. Guo was funded by the Recruitment Program of the Global Youth Experts of China, 2015. This research was supported by grants from the National Basic Research Program of China (grants 2013CB910102 and 2017YFA0503403), the National Science Foundation of China (grant 31230043 to C. Yang and grant 31671480 to Y. Jian), the Chinese Academy of Sciences Interdisciplinary Innovation Team to C. Yang, and the Chinese Academy of Sciences Key Research Program of Frontier Sciences (grant QYZDB-SSW-SMC046 to W. Guo).

The authors declare no competing financial interests.

Author contributions: C. Yang, K. Liu, and W. Guo conceived and designed this research. K. Liu, Y. Jing, and Z. Gao performed most of the cell biological and biochemical experiments and analyzed the data. R. Xing, K. Liu, and W. Guo performed animal experiments and analyzed the results. X. Ma, X. Sun, Y. Li, M. Xu, X. Wang, and Y. Jing contributed materials. C. Yang and W. Guo supervised the study. K. Liu, W. Guo, and C. Yang wrote the manuscript with feedback from all authors.

Submitted: 23 May 2017
Revised: 3 July 2017
Accepted: 12 July 2017

References

Ascano, M., D. Bodmer, and R. Kuruvilla. 2012. Endocytic trafficking of neurotrophins in neural development. *Trends Cell Biol.* 22:266–273. http://dx.doi.org/10.1016/j.tcb.2012.02.005

Barford, K., C. Deppmann, and B. Winckler. 2017. The neurotrophin receptor signaling endosome: Where trafficking meets signaling. *Dev. Neurobiol.* 77:405–418. http://dx.doi.org/10.1002/dneu.22427

BasuRay, S., S. Mukherjee, E. Romero, M.C. Wilson, and A. Wandinger-Ness. 2010. Rab7 mutants associated with Charcot-Marie-Tooth disease exhibit enhanced NGF-stimulated signaling. *PLoS One.* 5:e15351. http://dx.doi.org/10.1371/journal.pone.0015351

Cabrera, M., and C. Ungermann. 2010. Guiding endosomal maturation. *Cell.* 141:404–406. http://dx.doi.org/10.1016/j.cell.2010.04.013

Cabrera, M., M. Nordmann, A. Perz, D. Schmedt, A. Gerondopoulos, F. Barr, J. Piehler, S. Engelbrecht-Vandré, and C. Ungermann. 2014. The Mon1-Ccz1 GEF activates the Rab7 GTPase Ypt7 via a longin-fold-Rab interface and association with PI3P-positive membranes. *J. Cell Sci.* 127:1043–1051. http://dx.doi.org/10.1242/jcs.140921

Chen, D., Y. Jian, X. Liu, Y. Zhang, J. Liang, X. Qi, H. Du, W. Zou, L. Chen, Y. Chai, et al. 2013. Clathrin and AP2 are required for phagocytic receptor-mediated apoptotic cell clearance in *Caenorhabditis elegans. PLoS Genet.* 9:e1003517. http://dx.doi.org/10.1371/journal.pgen.1003517

Chotard, L., A.K. Mishra, M.A. Sylvain, S. Tuck, D.G. Lambright, and C.E. Rocheleau. 2010. TBC-2 regulates RAB-5/RAB-7-mediated endosomal trafficking in *Caenorhabditis elegans. Mol. Biol. Cell.* 21:2285–2296. http://dx.doi.org/10.1091/mbc.E09-11-0947

Christoforidis, S., M. Miaczynska, K. Ashman, M. Wilm, L. Zhao, S.C. Yip, M.D. Waterfield, J.M. Backer, and M. Zerial. 1999. Phosphatidylinositol-3-OH kinases are Rab5 effectors. *Nat. Cell Biol.* 1:249–252. http://dx.doi.org/10.1038/12075

Dove, S.K., K. Dong, T. Kobayashi, F.K. Williams, and R.H. Michell. 2009. Phosphatidylinositol 3,5-bisphosphate and Fab1p/PIKfyve underPPIn endo-lysosome function. *Biochem. J.* 419:1–13. http://dx.doi.org/10.1042/BJ20081950

Funderburk, S.F., Q.J. Wang, and Z. Yue. 2010. The Beclin 1-VPS34 complex--at the crossroads of autophagy and beyond. *Trends Cell Biol.* 20:355–362. http://dx.doi.org/10.1016/j.tcb.2010.03.002

Gillooly, D.J., I.C. Morrow, M. Lindsay, R. Gould, N.J. Bryant, J.M. Gaullier, R.G. Parton, and H. Stenmark. 2000. Localization of phosphatidylinositol 3-phosphate in yeast and mammalian cells. *EMBO J.* 19:4577–4588. http://dx.doi.org/10.1093/emboj/19.17.4577

Girard, E., D. Chmiest, N. Fournier, L. Johannes, J.L. Paul, B. Vedie, and C. Lamaze. 2014. Rab7 is functionally required for selective cargo sorting at the early endosome. *Traffic.* 15:309–326. http://dx.doi.org/10.1111/tra.12143

Hnia, K., I. Vaccari, A. Bolino, and J. Laporte. 2012. Myotubularin phosphoinositide phosphatases: cellular functions and disease pathophysiology. *Trends Mol. Med.* 18:317–327. http://dx.doi.org/10.1016/j.molmed.2012.04.004

Huotari, J., and A. Helenius. 2011. Endosome maturation. *EMBO J.* 30:3481–3500. http://dx.doi.org/10.1038/emboj.2011.286

Ikonomov, O.C., D. Sbrissa, and A. Shisheva. 2006. Localized PtdIns 3,5-P2 synthesis to regulate early endosome dynamics and fusion. *Am. J. Physiol. Cell Physiol.* 291:C393–C404. http://dx.doi.org/10.1152/ajpcell.00019.2006

Irannejad, R., N.G. Tsvetanova, B.T. Lobingier, and M. von Zastrow. 2015. Effects of endocytosis on receptor-mediated signaling. *Curr. Opin. Cell Biol.* 35:137–143. http://dx.doi.org/10.1016/j.ceb.2015.05.005

Johansson, M., N. Rocha, W. Zwart, I. Jordens, L. Janssen, C. Kuijl, V.M. Olkkonen, and J. Neefjes. 2007. Activation of endosomal dynein motors by stepwise assembly of Rab7-RILP-p150Glued, ORP1L, and the receptor βlll spectrin. *J. Cell Biol.* 176:459–471. http://dx.doi.org/10.1083/jcb.200606077

Kawauchi, T., K. Sekine, M. Shikanai, K. Chihama, K. Tomita, K. Kubo, K. Nakajima, Y. Nabeshima, and M. Hoshino. 2010. Rab GTPases-dependent endocytic pathways regulate neuronal migration and maturation through N-cadherin trafficking. *Neuron.* 67:588–602. http://dx.doi.org/10.1016/j.neuron.2010.07.007

Kelley, L.A., S. Mezulis, C.M. Yates, M.N. Wass, and M.J. Sternberg. 2015. The Phyre2 web portal for protein modeling, prediction and analysis. *Nat. Protoc.* 10:845–858. http://dx.doi.org/10.1038/nprot.2015.053

Li, W., W. Zou, D. Zhao, J. Yan, Z. Zhu, J. Lu, and X. Wang. 2009. *C. elegans* Rab GTPase activating protein TBC-2 promotes cell corpse degradation by regulating the small GTPase RAB-5. *Development.* 136:2445–2455. http://dx.doi.org/10.1242/dev.035949

Lindmo, K., and H. Stenmark. 2006. Regulation of membrane traffic by phosphoinositide 3-kinases. *J. Cell Sci.* 119:605–614. http://dx.doi.org/10.1242/jcs.02855

Liu, K., Y. Jian, X. Sun, C. Yang, Z. Gao, Z. Zhang, X. Liu, Y. Li, J. Xu, Y. Jing, et al. 2016. Negative regulation of phosphatidylinositol 3-phosphate levels in early-to-late endosome conversion. *J. Cell Biol.* 212:181–198. (published erratum appears in *J. Cell Biol. (Henderson NV).* 212:181–198.

Maritzen, T., H. Schachtner, and D.F. Legler. 2015. On the move: endocytic trafficking in cell migration. *Cell. Mol. Life Sci.* 72:2119–2134. http://dx.doi.org/10.1007/s00018-015-1855-9

McEwan, D.G., D. Popovic, A. Gubas, S. Terawaki, H. Suzuki, D. Stadel, F.P. Coxon, D. Miranda de Stegmann, S. Bhogaraju, K. Maddi, et al. 2015. PLEKHM1 regulates autophagosome-lysosome fusion through HOPS complex and LC3/GABARAP proteins. *Mol. Cell.* 57:39–54. http://dx.doi.org/10.1016/j.molcel.2014.11.006

Murray, J.T., C. Panaretou, H. Stenmark, M. Miaczynska, and J.M. Backer. 2002. Role of Rab5 in the recruitment of hVps34/p150 to the early endosome. *Traffic.* 3:416–427. http://dx.doi.org/10.1034/j.1600-0854.2002.30605.x

Nordmann, M., M. Cabrera, A. Perz, C. Bröcker, C. Ostrowicz, S. Engelbrecht-Vandré, and C. Ungermann. 2010. The Mon1-Ccz1 complex is the GEF of the late endosomal Rab7 homolog Ypt7. *Curr. Biol.* 20:1654–1659. http://dx.doi.org/10.1016/j.cub.2010.08.002

Numrich, J., and C. Ungermann. 2014. Endocytic Rabs in membrane trafficking and signaling. *Biol. Chem.* 395:327–333. http://dx.doi.org/10.1515/hsz-2013-0258

Pankiv, S., E.A. Alemu, A. Brech, J.A. Bruun, T. Lamark, A. Overvatn, G. Bjørkøy, and T. Johansen. 2010. FYCO1 is a Rab7 effector that binds to LC3 and PI3P to mediate microtubule plus end-directed vesicle transport. *J. Cell Biol.* 188:253–269. http://dx.doi.org/10.1083/jcb.200907015

Poteryaev, D., S. Datta, K. Ackema, M. Zerial, and A. Spang. 2010. Identification of the switch in early-to-late endosome transition. *Cell.* 141:497–508. http://dx.doi.org/10.1016/j.cell.2010.03.011

Press, B., Y. Feng, B. Hoflack, and A. Wandinger-Ness. 1998. Mutant Rab7 causes the accumulation of cathepsin D and cation-independent mannose 6-phosphate receptor in an early endocytic compartment. *J. Cell Biol.* 140:1075–1089. http://dx.doi.org/10.1083/jcb.140.5.1075

Raiborg, C., E.M. Wenzel, N.M. Pedersen, H. Olsvik, K.O. Schink, S.W. Schultz, M. Vietri, V. Nisi, C. Bucci, A. Brech, et al. 2015. Repeated ER-endosome contacts promote endosome translocation and neurite outgrowth. *Nature.* 520:234–238. http://dx.doi.org/10.1038/nature14359

Renault, L., J. Kuhlmann, A. Henkel, and A. Wittinghofer. 2001. Structural basis for guanine nucleotide exchange on Ran by the regulator of chromosome condensation (RCC1). *Cell.* 105:245–255. http://dx.doi.org/10.1016/S0092-8674(01)00315-4

Rink, J., E. Ghigo, Y. Kalaidzidis, and M. Zerial. 2005. Rab conversion as a mechanism of progression from early to late endosomes. *Cell.* 122:735–749. http://dx.doi.org/10.1016/j.cell.2005.06.043

Schink, K.O., C. Raiborg, and H. Stenmark. 2013. Phosphatidylinositol 3-phosphate, a lipid that regulates membrane dynamics, protein sorting and cell signalling. *BioEssays.* 35:900–912.

Shinde, S.R., and S. Maddika. 2016. PTEN modulates EGFR late endocytic trafficking and degradation by dephosphorylating Rab7. *Nat. Commun.* 7:10689. http://dx.doi.org/10.1038/ncomms10689

Spinosa, M.R., C. Progida, A. De Luca, A.M. Colucci, P. Alifano, and C. Bucci. 2008. Functional characterization of Rab7 mutant proteins associated with Charcot-Marie-Tooth type 2B disease. *J. Neurosci.* 28:1640–1648. http://dx.doi.org/10.1523/JNEUROSCI.3677-07.2008

Stein, M.P., Y. Feng, K.L. Cooper, A.M. Welford, and A. Wandinger-Ness. 2003. Human VPS34 and p150 are Rab7 interacting partners. *Traffic.* 4:754–771. http://dx.doi.org/10.1034/j.1600-0854.2003.00133.x

Stein, M.P., C. Cao, M. Tessema, Y. Feng, E. Romero, A. Welford, and A. Wandinger-Ness. 2005. Interaction and functional analyses of human VPS34/p150 phosphatidylinositol 3–kinase complex with Rab7. *Methods Enzymol.* 403:628–649. http://dx.doi.org/10.1016/S0076-6879(05)03055-7

Stenmark, H., and D.J. Gillooly. 2001. Intracellular trafficking and turnover of phosphatidylinositol 3-phosphate. *Semin. Cell Dev. Biol.* 12:193–199. http://dx.doi.org/10.1006/scdb.2000.0236

Stirnimann, C.U., E. Petsalaki, R.B. Russell, and C.W. Müller. 2010. WD40 proteins propel cellular networks. *Trends Biochem. Sci.* 35:565–574. http://dx.doi.org/10.1016/j.tibs.2010.04.003

Tang, B.L. 2008. Emerging aspects of membrane traffic in neuronal dendrite growth. *Biochim. Biophys. Acta.* 1783:169–176. http://dx.doi.org/10.1016/j.bbamcr.2007.11.011

Vonderheit, A., and A. Helenius. 2005. Rab7 associates with early endosomes to mediate sorting and transport of Semliki forest virus to late endosomes. *PLoS Biol.* 3:e233. http://dx.doi.org/10.1371/journal.pbio.0030233

Wang, Z., G. Miao, X. Xue, X. Guo, C. Yuan, Z. Wang, G. Zhang, Y. Chen, D. Feng, J. Hu, and H. Zhang. 2016. The Vici syndrome protein EPG5 is a Rab7 effector that determines the fusion specificity of autophagosomes with late endosomes/lysosomes. *Mol. Cell.* 63:781–795. http://dx.doi.org/10.1016/j.molcel.2016.08.021

Wurmser, A.E., and S.D. Emr. 1998. Phosphoinositide signaling and turnover: PtdIns(3)P, a regulator of membrane traffic, is transported to the vacuole and degraded by a process that requires lumenal vacuolar hydrolase activities. *EMBO J.* 17:4930–4942. http://dx.doi.org/10.1093/emboj/17.17.4930

Yap, C.C., and B. Winckler. 2012. Harnessing the power of the endosome to regulate neural development. *Neuron.* 74:440–451. http://dx.doi.org/10.1016/j.neuron.2012.04.015

Zhong, Y., Q.J. Wang, X. Li, Y. Yan, J.M. Backer, B.T. Chait, N. Heintz, and Z. Yue. 2009. Distinct regulation of autophagic activity by Atg14L and Rubicon associated with Beclin 1-phosphatidylinositol-3-kinase complex. *Nat. Cell Biol.* 11:468–476. http://dx.doi.org/10.1038/ncb1854